Nanosecond Random Telegraph Noise in In-Plane Magnetic Tunnel Junctions

K. Hayakawa, S. Kanai, T. Funatsu, J. Igarashi, B. Jinnai, W. A. Borders, H. Ohno, and S. Fukami

Phys. Rev. Lett. **126**, 117202 — Published 17 March 2021

DOI: 10.1103/PhysRevLett.126.117202

Nanosecond random telegraph noise in in-plane magnetic tunnel junctions

K. Hayakawa,[1] S. Kanai,[1-4,*] T. Funatsu,[1] J. Igarashi,[1] B. Jinnai,[5] W. A. Borders,[1] H. Ohno,[1,3-6] and S. Fukami[1,3-6]

[1]Laboratory for Nanoelectronics and Spintronics, Research Institute of Electrical Communication, Tohoku University, Sendai 980-8577, Japan

[2]Division for the Establishment of Frontier Sciences, Organization for Advanced Studies, Tohoku University, Sendai 980-8577, Japan

[3]Center for Spintronics Research Network, Tohoku University, Sendai 980-8577, Japan

[4]Center for Science and Innovation in Spintronics, Tohoku University, Sendai 980-8577, Japan

[5]WPI-Advanced Institute for Materials Research, Tohoku University, Sendai 980-8577, Japan

[6]Center for Innovative Integrated Electronic Systems, Tohoku University, Sendai 980-0845, Japan

*e-mail: skanai@tohoku.ac.jp

ABSTRACT

We study the timescale of random telegraph noise (RTN) of nanomagnets in stochastic magnetic tunnel junctions (MTJs). From analytical and numerical calculations based on the Landau-Lifshitz-Gilbert and the Fokker-Planck equations, we reveal mechanisms governing the relaxation time of perpendicular easy-axis MTJs (p-MTJs) and in-plane easy-axis MTJs (i-MTJs), showing that i-MTJs can be made to have faster RTN. Superparamagnetic i-MTJs with small in-plane anisotropy and sizable perpendicular effective anisotropy show relaxation times down to 8 ns at negligible bias current, which is more than five-orders-of-magnitude shorter than that of typical stochastic p-MTJs and about 100-times faster than the shortest time of i-MTJs reported so far. The findings give a new insight and foundation in developing stochastic MTJs for high-performance probabilistic computers.

Unraveling the physical mechanisms underlying probabilistic behavior has grown increasingly important as stochastic physical systems are being recognized as a useful ingredient for unconventional computing [1,2]. Thermally-stable magnetic tunnel junctions (MTJs) have been established as a critical building block for low-power, non-volatile integrated circuits. Recently, thermally-unstable MTJs on the opposite extreme, showing a stochastic magnetization configuration, or random telegraph noise (RTN), have also started to gather attention as a key enabler for probabilistic computers initially envisioned by Feynman [2-13]. Here, the fluctuation timescale, or the Néel relaxation time, of the MTJs is a crucial factor for determining performance, where a shorter relaxation time yields a faster time-to-solution and higher precision. A proof-of-concept of integer factorization was demonstrated using a rudimentary system with perpendicular-anisotropy MTJs (p-MTJs) whose typical relaxation time is in the millisecond range [2]. Meanwhile, in in-plane easy-axis MTJs (i-MTJs), relaxation times down to sub-microsecond have been reported [4,9,14-17], several orders of magnitude shorter than that of p-MTJs [2,18]. Importantly, while vigorous efforts have been dedicated to the long-term retention property of nonvolatile MTJs [19-27], the physical mechanism governing the relaxation time of stochastic MTJs has not been well studied. Accordingly, the present understanding cannot account for the largely different relaxation times in the two systems with different easy-axis directions, and thus is unable to present effective approaches to reduce the relaxation time of stochastic MTJs. Here, we introduce free energy for qualitative description of the stochasticity and find that faster precession caused by the sizable perpendicular anisotropy of i-MTJ enables to achieve shorter relaxation time. We experimentally investigate the RTN of i-MTJs which show a short relaxation time down to 8 ns at negligible bias current. We also perform numerical calculations and clarify the mechanism that is responsible for the shorter relaxation time of i-MTJs than that of p-MTJs. In a joint publication article [28], we thoroughly describe the formalism and mechanism of the relaxation time of stochastic nanomagnets with perpendicular and in-plane easy axes.

A stack structure consisting of Ta (5 nm)/ PtMn (20 nm)/ Co (2.6 nm)/ Ru (0.9 nm)/ CoFeB

(2.4 nm)/ MgO/ CoFeB (t_{free})/ Ta (5 nm)/ Ru (5 nm) is deposited on a thermally oxidized Si substrate by dc/rf magnetron sputtering at room temperature (Fig. 1(a)). The bottom CoFeB layer is a reference layer with an in-plane magnetic easy axis, and shows antiferromagnetic coupling with the Co layer that is pinned by PtMn. The free layer CoFeB with thickness t_{free} = 2.1 nm also possesses an in-plane easy axis. The effective perpendicular anisotropy field $\mu_0 H_K^{eff}$ is determined to be -0.46 T (μ_0 is the permeability in free space and minus sign indicates an in-plane easy axis) from magnetization curve measurements using vibrating sample magnetometry (VSM). The stack is processed into elliptical MTJs with electron-beam lithography, reactive-ion etching, and Ar-ion milling. Then, co-planar waveguide made of Cr (5 nm)/ Au (100 nm) is formed by Ar-ion milling. The samples are annealed at 300°C for two hours in vacuum with an external magnetic field $\mu_0 H_{in}$ of 1.2 T parallel to the in-plane easy axis (long axis) to provide the exchange bias. The resistance area product RA is determined to be 32±2 Ωμm^2 from the area determined by the scanning electron microscope (SEM) image and junction resistance of 113 reference MTJs with different dimensions. Tunnel magnetoresistance (TMR) ratio is 110±12%. Figure 1(b) shows a SEM image of the elliptical MTJ having the device size and aspect ratio of 104 nm × 149 nm and 1.4, respectively. In this paper, we show the results of three MTJ devices (A, B, and C) with the same design. All experiments are conducted under a magnetic field H_{in} parallel to the easy axis of the MTJs. Figure 1(c) shows the R-H_{in} curve of the MTJ devices A-C with schematics of expected energy potential. Differences in resistance (~20%) and shift field $\mu_0 H_S$ (~3 mT) between them reflect the deviation of the fabricated MTJ dimension. A superparamagnetic behavior with zero coercivity is observed, indicating event time τ is well below the measurement time (~1 second) for all devices.

Figure 2(a) shows the circuit configuration for the RTN measurement down to sub-nanosecond event times. A small dc voltage V_{dc} = 0.1 V, corresponding to the current and current density of 19 μA and 0.31×10^6 A/cm^2, is applied to the MTJ. The applied current is negligibly

small compared to the critical current (~8%), suggesting spin-transfer torque does not play major roles, as is experimentally supported by the fact that V_{dc} with the opposite polarity does not exhibit any change in the following measurement. High-frequency transmitted signal is monitored by a high-speed oscilloscope. A bias tee with cut-on frequency >100 kHz is used to shunt the dc component of the voltage applied to the oscilloscope/amplifier. Figure 2(b)-(d) shows the typical time-resolved RTN signal with $\mu_0 H_{in}$ = -8.6 mT, -7.9 mT, and -7.4 mT, respectively. Due to the TMR effect, the high-frequency transmission coefficient $\Gamma(R) = 2Z_0/(Z_0 + R)$ and resultant transmission voltage $V_T(R) = V_{dc}\Gamma(R)A_V$ change with the magnetic configuration [29], where Z_0 is the characteristic impedance of the circuit 50 Ω, and A_V the gain of the inverter amplifier $-20\log 15$. The difference of RTN signal for parallel (P) and antiparallel (AP) configurations is calculated to be $V_T(R_{AP}) - V_T(R_P) = 9.4$ mV, using the resistances under P and AP configurations (R_P and R_{AP}), respectively, for device A. This value agrees with the experimentally obtained RTN signal amplitude ~ 9 mV shown in Figs. 2(b)-(d), indicating that 180° switching between P and AP states takes place. As indicated in Fig. 2(c), we measure each event time t_{event} by measuring the time between subsequent magnetization switching events. Figure 2(e) shows an example of the histogram of t_{event} determined from RTN measurements over 4 ms. The number of the event time N shows a typical exponential distribution $N = \tau^{-1}\exp(-t_{event}/\tau)$, indicating the switching event follows a Poisson process. The expectation values of event time (= relaxation time) τ is determined by fitting an exponential function to the experimental result shown in the solid lines in Fig. 2(e).

As shown in Figs. 2(b)-(d), τ_P and τ_{AP} change with H_{in} due to a modulation of the energy potential. At $\mu_0 H_{in} = -7.9$ mT, $\tau_P \approx \tau_{AP}$ as shown in Figs. 2(c), which is also consistent with the center of the $R - H_{in}$ curve (Fig. 1(c)). Figures 2(f) and 2(g) are the RTN of the devices B and C taken at H_{in} with $\tau_P \approx \tau_{AP}$, respectively. Difference in the H_{in} originates from different uncompensated stray fields H_S from the reference layer due to the deviation of fabricated MTJ dimensions. Figure 3 summarizes τ_P and τ_{AP} as a function of H_{in} for devices

A-C. We define the averaged relaxation time as $\tau_{\mathrm{ave}} \equiv \sqrt{\tau_{\mathrm{P}}\tau_{\mathrm{AP}}}$. The lowest τ_{ave} is 8 ns, which is five orders shorter than that of typical p-MTJs [2,18], and more than 100 times shorter than the shortest value ever demonstrated in i-MTJs (980 ns) [17].

Now we analyze the obtained results from a relation of the relaxation time with H_{in}. Magnetic energy density $f(\theta,\varphi)$ per magnetic moment $M_{\mathrm{S}}V$ under perpendicular uniaxial magnetic anisotropy, in-plane uniaxial magnetic anisotropy, and H_{in} is expressed as

$$f(\theta,\varphi) = -H_{\mathrm{in}}\sin\theta\cos\varphi + \frac{1}{2}H_K^{\mathrm{eff}}\sin^2\theta + \frac{1}{2}H_{K,\mathrm{in}}\sin^2\theta\sin^2\varphi, \tag{1}$$

where (θ,φ), $H_{K,\mathrm{in}}$, M_{S}, and V are polar and azimuthal angles of the free layer magnetization, in-plane anisotropy field, spontaneous magnetization, and volume of the free layer, respectively. We define $\theta = 0$ as the perpendicular $(+z)$ direction, and $(\theta,\varphi) = (\pi/2, 0)$ as the long axis $(+x)$ direction. In general, the in-plane energy barrier $E_{\mathrm{P(AP)}}$ from P to AP (AP to P) process is known to be given by

$$E_{\mathrm{P(AP)}} = \frac{\left[H_{K,\mathrm{in}} + (-)\{H_{\mathrm{in}} - H_{\mathrm{S}}\}\right]^2}{2H_{K,\mathrm{in}}}M_{\mathrm{S}}V. \tag{2}$$

In the Néel-Arrhenius law, the relaxation time of the P and AP states are $\tau_{\mathrm{P(AP)}} = \tau_0\exp\left(E_{\mathrm{P(AP)}}/k_{\mathrm{B}}T\right)$, where τ_0, k_{B}, and T are the attempt time, Boltzmann constant, and temperature, respectively [30]. On the logarithmic scale,

$$\ln\tau_{\mathrm{P(AP)}} \approx \frac{M_{\mathrm{S}}V}{2k_{\mathrm{B}}T}\left[+(-)2\{H_{\mathrm{in}} - H_{\mathrm{S}}\} + H_{K,\mathrm{in}}\right] + \ln\tau_0 \tag{3}$$

at $|H_{\mathrm{in}} - H_{\mathrm{S}}| \ll H_{K,\mathrm{in}}$. The term of $\frac{M_{\mathrm{S}}V}{2k_{\mathrm{B}}T}[\pm 2H_{\mathrm{in}}]$ governs the slope and the rest determines the offset. Fitting Eq. (3) to the data at $\tau_{\mathrm{P}} \approx \tau_{\mathrm{AP}}$ for device A shown in Fig. 3, we obtain $M_{\mathrm{S}}V = (1.3\pm0.1)\times10^{-23}$ Tm^3 from the slope $\pm M_{\mathrm{S}}V/k_{\mathrm{B}}T$, which corresponds to about 60% of the value of $M_{\mathrm{S}}t_{\mathrm{free}}A = (2.3\pm0.2)\times10^{-23}$ Tm^3, where the areal magnetic moment $M_{\mathrm{S}}t_{\mathrm{free}}$ is determined from the VSM measurements and A from the RA divided by junction resistance of device A. The reasonable agreement indicates that the studied system can be approximated by a single-domain

model although the switching is driven with an activation volume slightly smaller than the entire volume of the free layer.

In the following section, we theoretically study the relaxation time of the p- and i-MTJs, and discuss the mechanism which yields the fast relaxation time in i-MTJs [28]. First, we compare the relaxation time of the two configurations with a macrospin model using the Landau-Lifshitz-Gilbert (LLG) equation,

$$\frac{\mathrm{d}\boldsymbol{m}}{\mathrm{d}t} = -\gamma\mu_0\boldsymbol{m}\times\left(\boldsymbol{\nabla}f + \boldsymbol{h}_{\mathrm{T}}(t)\right) + \alpha\boldsymbol{m}\times\frac{\mathrm{d}\boldsymbol{m}}{\mathrm{d}t}, \tag{4}$$

where $\boldsymbol{m} = (\sin\theta\cos\varphi, \sin\theta\sin\varphi, \cos\theta)$, t, γ, $\boldsymbol{h}_{\mathrm{T}}(t)$, and α are the normalized magnetization vector, time, gyromagnetic ratio, random thermal field vector, and damping constant, respectively. $f(\theta,\varphi)$ is defined in Eq. (1). We define the initial magnetization direction of p-MTJs (i-MTJs) at $\theta = 0 \Leftrightarrow m_z = 1$ ($(\theta,\varphi) = (\pi/2,0) \Leftrightarrow m_x = 1$).

For the p-MTJs, Fig. 4(a) illustrates the direction of each torque in Eq. (4). Importantly, thermal fluctuations are isotropic and its polar component is the only driving force to induce magnetization switching among the torques. We numerically calculate the time evolution of magnetization using Eq. (4) with α =0.02 and $\mu_0 H_K^{\mathrm{eff}}$ =10 mT, corresponding to the thermal stability factor $\Delta \equiv M_S H_K^{\mathrm{eff}} V/2k_{\mathrm{B}}T$ = 3.8 at T = 300 K for a magnet with the thickness and diameter of 1 nm and 60 nm, respectively. As shown in Fig. 4(b), magnetization dynamics are dominated by the precession towards azimuthal direction resulting from the anisotropy field, and the thermal field towards polar direction changes precession radius. Figure 4(c) shows z component m_z of the magnetization *vs*. time, showing an event time on the order of microseconds. Averaging 10,000 event time, we obtain the relaxation time for this configuration to be 0.80 μs.

For i-MTJs, Fig. 4(f) illustrates the direction of torques in Eq. (4) at $\varphi = 0$. In i-MTJs with a thermal fluctuation field, once the magnetization acquires an out-of-plane component ($m_z > 0$), the perpendicular component of magnetic anisotropy generates a strong torque $\dot{\varphi}\sim\gamma\mu_0 H_K^{\mathrm{eff}}\cos\theta$

unlike p-MTJs. With an increase of φ, the magnetization returns to the plane ($\theta = \pi/2$) due to the torque from $H_{K,\mathrm{in}}$, $\dot{\theta} \sim \gamma \mu_0 H_{K,\mathrm{in}} \sin\theta \sin 2\varphi$, while conserving the potential energy, resulting in magnetization precession with an elliptic trajectory about the energy minimum. Figures 4(g) and 4(h) show the calculated magnetization trajectory with $\mu_0 H_{K,\mathrm{in}} = 10$ mT ($\Delta \equiv M_\mathrm{S} H_{K,\mathrm{in}} V / 2k_\mathrm{B}T = 3.8$), $\mu_0 H_K^{\mathrm{eff}} = -460$ mT, and $\alpha = 0.02$. As shown in Fig. 4(g), the magnetization precesses along elliptic orbits, changing its radius by thermal fluctuation. Figure 4(h) shows x component m_x of the magnetization *vs*. time, showing an event time on the order of tens of nanoseconds. The relaxation time obtained from 10,000 switching events is 20 ns, which is in good agreement with the experimentally observed relaxation times (Fig. 3). It is noteworthy that despite the same Δ of 3.8 between the p- and i-MTJs, the numerically calculated relaxation times are different by a factor of 40.

Figures 4(d) and 4(i) show the contour map of the potential energy density $f(\theta, \varphi) M_\mathrm{S} V$ for p- and i-MTJs, respectively. Black and gray lines show the contour spacing of $1k_\mathrm{B}T$ and $20k_\mathrm{B}T$, respectively. Potential energy is indicated by color as well, whose scale is shown in Figs. 4(e) and 4(j). In p-MTJs [Figs. 4(d),(e)], the potential landscape is simply composed of two energy valleys separated by barrier energy at the equator $\theta = \pi/2$, where the energy takes the maximum value in all directions (θ, φ). On the contrary, in i-MTJs [Figs. 4(i),(j)], two energy valleys are surrounded by high energy regions due to a relatively large $|H_K^{\mathrm{eff}}|$ and are connected at two saddle points $(\theta, \varphi) = (\pi/2, \pm\pi/2)$ on the equator at which energy is $3.8k_\mathrm{B}T$. Accordingly, the magnetization is confined in the relatively low energy region at the vicinity of the in-plane direction as shown in Fig. 4(g).

In a joint publication article [28], we investigate the mechanism of thermally activated switching numerically and analytically based on the LLG equation above and the Fokker-Planck (FP) equation, which describes the time evolution of the probability density $P(t, \theta, \varphi)$ to take magnetization direction (θ, φ). The analytical investigation reveals that the decay time that non-

equilibrium $P(t,\ \theta,\ \varphi)$ relaxes to equilibrium (Boltzmann) distribution is shorter for a larger gradient of potential landscape $|\boldsymbol{\nabla} f| = |\boldsymbol{m} \times \boldsymbol{\nabla} f|$; in other words, faster intrinsic precessional frequency induces shorter relaxation time. In i-MTJs, the precession frequency at the bottom of the energy valley is given by $\gamma\mu_0\left(-H_K^{\mathrm{eff}}H_{K,\mathrm{in}}\right)^{0.5}$ rad/s, which is much faster than that of p-MTJs $\gamma\mu_0 H_{K,\mathrm{in}}$ rad/s. In i-MTJs, because the gradient of potential landscape is larger than p-MTJs and finite at anywhere except for two saddle points, the magnetization always feels non-zero torque $\boldsymbol{m} \times \boldsymbol{\nabla} f$ that drives the switching in addition to the diffusion of the probability density, which is visualized as the rapid spread of $P(t,\ \theta,\ \varphi)$ from original energy valley to the other using numerical simulation with the FP equation. This is in contrast to the case of p-MTJs, where magnetization feels zero torque at the vicinity of the energy barrier because $\boldsymbol{\nabla} f = 0$, and the switching takes place only by the probability density diffusion through the random walk. This difference reasonably accounts for the different timescales in τ for the i-MTJs and p-MTJs even with the same Δ.

In thermally stable MTJs, their year-long τ is not easily accessed with experiments and numerical simulations. Due to this limitation, the most effective way to increase (decrease) τ has been believed to increase (decrease) Δ by increasing (decreasing) the energy barrier, considering the Néel-Arrhenius law $\tau = \tau_0 \exp(\Delta)$, assuming a constant τ_0 = 1 ns. A theoretical study was performed on the basis of this understanding and Δ = 0 is assumed for analytical and numerical calculations [31]. In this Letter and the joint publication article [28], we directly access τ by measuring RTN of stochastic MTJs and perform analytical and numerical calculations while assuming a finite Δ, reaching the following understandings. The difference in the dynamics indicates that τ_0 significantly changes with the magnetic anisotropy configuration because τ_0 is determined by the intrinsic precessional frequency. Accordingly, in p-MTJs, the reduction of Δ is not an efficient approach to reduce τ due to the increase of τ_0 with a decrease of Δ, and there is a lower limit of τ which is determined by α and $M_S V$. In i-MTJs, on the other hand, τ_0 is

always smaller than that in p-MTJs for the same Δ, and can be reduced by a few orders of magnitude with changing the *perpendicular* effective anisotropy field, which does not have any contribution to Δ. These findings as well as the experimental results in this paper pave an effective way to control relaxation time.

In conclusion, we have investigated the relaxation time of the magnetization in stochastic in-plane easy-axis magnetic tunnel junctions (i-MTJs). From measurements on the random telegraph noise, we have obtained relaxation times down to 8 ns at negligibly small bias current, which is five orders of magnitude shorter than that of typical perpendicular MTJs (p-MTJs), and more than 100 times shorter than that reported for the i-MTJs so far. Numerical simulation reproduced the trend that i-MTJs have faster precession and shorter relaxation time than those with the p-MTJs even with the same thermal stability factor. Due to the difference of potential landscape formed by relatively large effective perpendicular anisotropy field, the probability density much more rapidly transits to the other potential valley in i-MTJs. The experimental results and model in the joint publication article [28] give a compass for designing stochastic MTJs with shorter relaxation time and benefits for probabilistic computer with faster operation time and higher precision.

During the preparation of this manuscript, we have learned that a similar manuscript is recently posted in arXiv [32], where auto-correlation time of junction resistance of an i-MTJ down to 2 ns was shown under a relatively large 7.0×10^6 A/cm^2.

ACKNOWLEDGMENTS.

The authors thank C. Igarashi and I. Morita for technical support. This work was supported in part by the JST-CREST No. JP1082016, JSPS Kakenhi Grant numbers 19J12206, 19J12926,

19H05622, 20H02178, and 19KK0130, and Cooperative Research Projects of RIEC. J.I. acknowledges GP-Spin of Tohoku University, and J.I. and W.A.B. acknowledge JST-OPERA for financial support.

REFERENCES

[1] R. P. Feynman, Int. J. Theor. Phys. **21**, 467 (1982).

[2] W. A. Borders, A. Z. Pervaiz, S. Fukami, K. Y. Camsari, H. Ohno, and S. Datta, Nature (London) **573**, 390 (2019).

[3] K. Y. Camsari, R. Faria, B. M. Sutton, and S. Datta, Phys. Rev. X **7**, 031014 (2017).

[4] M. Bapna and S. A. Majetich, Appl. Phys. Lett. **111**, 243107 (2017).

[5] K. Y. Camsari, S. Salahuddin, and S. Datta, IEEE Electron Device Lett. **38**, 1767 (2017).

[6] R. Faria, K. Y. Camsari, and S. Datta, IEEE Magn. Lett. **8**, 4105305 (2017).

[7] B. Sutton, K. Y. Camsari, B. Behin-Aein, and S. Datta, Sci. Rep. **7**, 44370 (2017).

[8] D. Vodenicarevic *et al.*, Phys. Rev. Appl. **8**, 054045 (2017).

[9] A. Mizrahi, T. Hirtzlin, A. Fukushima, H. Kubota, S. Yuasa, J. Grollier, and D. Querlioz, Nat. Commun. **9**, 1533 (2018).

[10] B. Parks, M. Bapna, J. Igbokwe, H. Almasi, W. G. Wang, and S. A. Majetich, AIP Adv. **8**,

055903 (2018).

[11] Y. Lv, R. P. Bloom, and J. P. Wang, IEEE Magn. Lett. **10**, 4510905 (2019).

[12] P. Debashis, R. Faria, K. Y. Camsari, S. Datta, and Z. Chen, Phys. Rev. B **101**, 094405 (2020).

[13] P. Debashis, V. Ostwal, R. Faria, S. Datta, J. Appenzeller, and Z. Chen, Sci. Rep. **10**, 16002 (2020).

[14] D. I. Suh, G. Y. Bae, H. S. Oh, and W. Park, J. Appl. Phys. **117**, 17D714 (2015).

[15] B. R. Zink, Y. Lv, and J.-P. Wang, J. Appl. Phys. **124**, 152121 (2018).

[16] Y. Lv, R. P. Bloom, and J. Wang, IEEE Magn. Lett. **10**, 4510905 (2019).

[17] B. Parks, A. Abdelgawad, T. Wong, R. F. L. Evans, and S. A. Majetich, Phys. Rev. Appl. **13**, 014063 (2020).

[18] J. L. G. Reiss, and K. Rott, Arxiv, 1908.02139v3 (2019).

[19] K. Watanabe, B. Jinnai, S. Fukami, H. Sato, and H. Ohno, Nat. Commun. **9**, 663 (2018).

[20] S. Ikeda *et al.*, Nat. Mater. **9**, 721 (2010).

[21] D. C. Worledge *et al.*, Appl. Phys. Lett. **98**, 022501 (2011).

[22] M. Gajek *et al.*, Appl. Phys. Lett. **100**, 132408 (2012).

[23] W. Kim *et al.*, in *International Electron Devices Meeting* 2011), p. 24.1.1.

[24] H. Sato, M. Yamanouchi, S. Ikeda, S. Fukami, F. Matsukura, and H. Ohno, Appl. Phys. Lett. **101**, 022414 (2012).

[25] G. Jan, Y. J. Wang, T. Moriyama, Y. J. Lee, M. Lin, T. Zhong, R. Y. Tong, T. Torng, and P. K. Wang, Appl Phys Express **5**, 093008 (2012).

[26] L. Thomas *et al.*, J. Appl. Phys. **115**, 172615 (2014).

[27] N. Perrissin *et al.*, Nanoscale **10**, 12187 (2018).

[28] S. Kanai, K. Hayakawa, S. Fukami, and H. Ohno, Jointly submitted to Phys. Rev. B**.**

[29] S. Kanai, M. Gajek, D. C. Worledge, F. Matsukura, and H. Ohno, Appl. Phys. Lett. **105**, 242409 (2014).

[30] L. Neel, Ann. Geophys. **5**, 99 (1949).

[31] J. Kaiser, A. Rusagi, K.Y. Camsari, J.Z. Sun, S. Datta, and P. Upadhyaya, Phys. Rev. Appl. **12**, 054056 (2019).

[32] C. Safranski, J. Kaiser, P. Trouilloud, P. Hashemi, G. Hu, and J. Z. Sun, Arxiv, 2010.14393 (2020).

FIGURE CAPTIONS

FIG. 1. Device design and basic device properties. (a) Schematic of stack structure. (b) Scanning microscope image of elliptic magnetic tunnel junction (MTJ). (c) Junction resistance R versus in-plane external magnetic field $\mu_0 H_{\text{in}}$ parallel to the easy axis of the MTJ.

FIG. 2. Random telegraph noise (RTN) measurements. (a) Circuit configuration of RTN measurements. (b)-(d) Measured RTN signals for (b) $\mu_0 H_{\text{in}}$ = -8.9 mT, (c) $\mu_0 H_{\text{in}}$ = -7.9 mT, (d) $\mu_0 H_{\text{in}}$ = -7.4 mT with device A. (e) Histogram of the event time t_{event} for P and AP states, analyzed at $\mu_0 H_{\text{in}}$ = -7.9 mT collected by monitoring RTN signal for 4 ms. (f),(g) Measured RTN signals for device B and C, respectively.

FIG. 3. In-plane magnetic field $\mu_0 H_{\text{in}}$ dependence of relaxation time for P and AP configurations, τ_{P} and τ_{AP}, respectively.

FIG. 4. Thermally activated magnetization switching for (a)-(e) p-MTJs and (f)-(j) i-MTJs with the same thermal stability factor $\Delta = 3.8$. For p-MTJs, perpendicular effective anisotropy field $\mu_0 H_K^{\text{eff}}$ = 10 mT, and for i-MTJs, in-plane effective anisotropy field $\mu_0 H_{K,\text{in}}$ = 10 mT, and $\mu_0 H_K^{\text{eff}}$ = -0.46 T are used to serve the same Δ in both configurations. (a)(f) Schematics of direction of

the torque. (b),(c),(g),(h) Magnetization dynamics simulated by LLG equation (Eq. (2)). Magnetization trajectories with duration of (b) 2 μs and (g) 50 ns are plotted. (d),(i) Potential energy landscapes described by Eq. (1). (e),(j) Schematics of the thermally activated magnetization switching between potential valley over energy barrier. White arrow in (d),(e),(i),(j) indicates the energy from bottom of the potential valley and barrier between potential valleys. Yellow arrow in (i),(j) indicates the energy from bottom of the potential valley and perpendicular direction ($m_z = 1$).

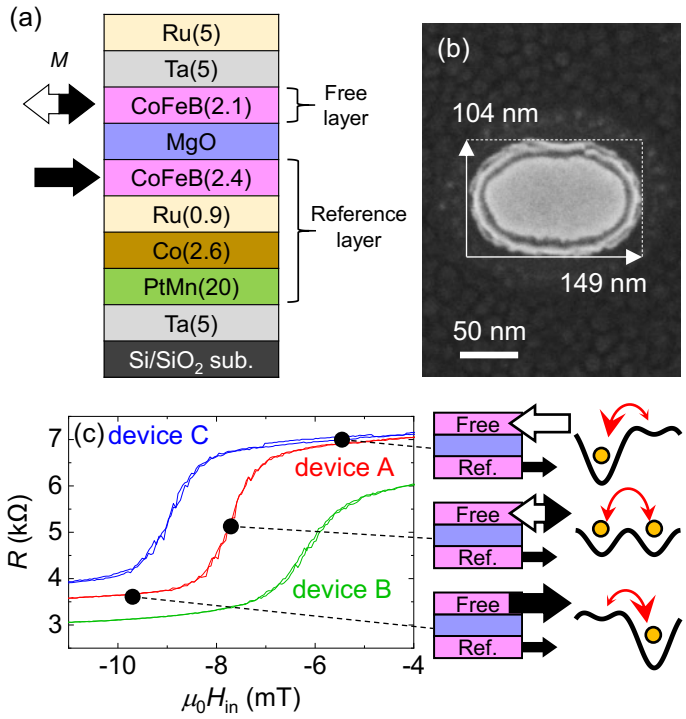
(a)
M
Ru(5)
Ta(5)
CoFeB(2.1)
MgO
CoFeB(2.4)
Ru(0.9)
Co(2.6)
PtMn(20)
Ta(5)
Si/SiO2 sub.
Free layer
Reference layer
(b)
104 nm
149 nm
50 nm
(c)
device C
device A
device B
R (kΩ)
μ0Hin (mT)
Free
Ref.

Fig. 1

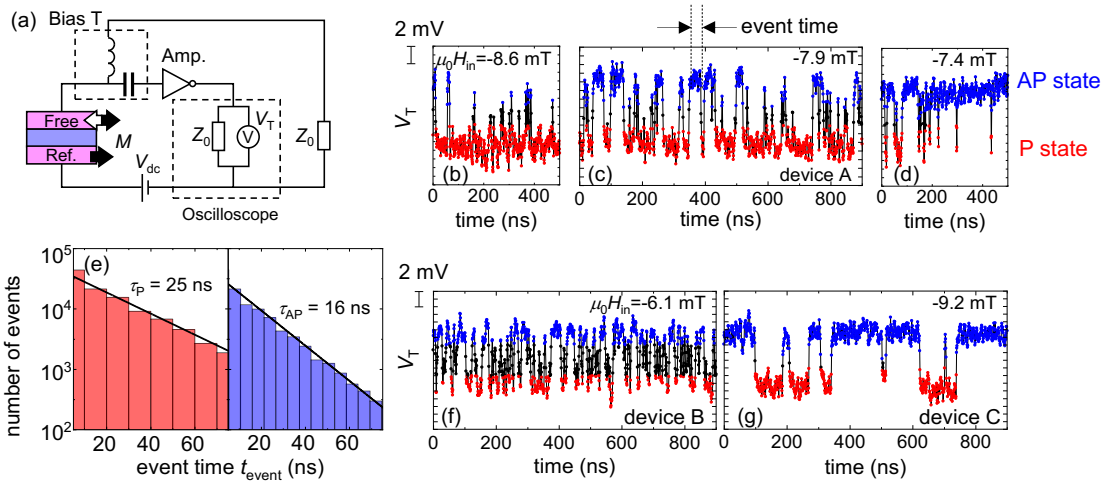
(a) Bias T
Amp.
Free
Ref.
M
V_{dc}
Z_0
V_T
Z_0
Oscilloscope
2 mV
event time
$\mu_0 H_{in}$=-8.6 mT
-7.9 mT
-7.4 mT
AP state
P state
(b)
(c)
device A
(d)
time (ns)
number of events
(e)
τ_P = 25 ns
τ_{AP} = 16 ns
event time t_{event} (ns)
2 mV
$\mu_0 H_{in}$=-6.1 mT
-9.2 mT
(f)
device B
(g)
device C
time (ns)

Fig. 2

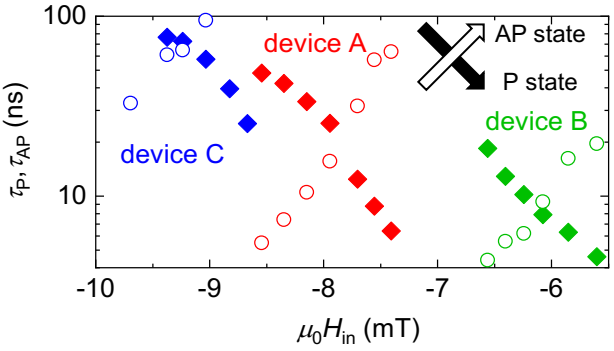
100
10
-10
-9
-8
-7
-6
τ_P, τ_{AP} (ns)
$\mu_0 H_{in}$ (mT)
device A
device B
device C
AP state
P state

Fig. 3

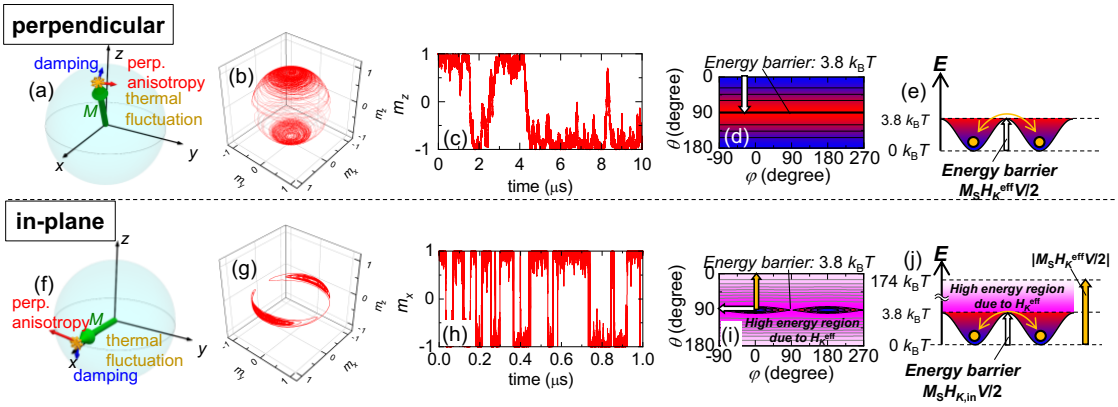
perpendicular
damping
perp.
anisotropy
thermal
fluctuation
(a)
M
z
y
x
(b)
(c)
time (μs)
Energy barrier: 3.8 k_BT
(d)
θ (degree)
φ (degree)
(e)
E
3.8 k_BT
0 k_BT
Energy barrier
$M_S H_K^{eff} V/2$
in-plane
(f)
perp.
anisotropy
thermal
fluctuation
damping
(g)
(h)
time (μs)
Energy barrier: 3.8 k_BT
(i)
High energy region
due to H_K^{eff}
(j)
$|M_S H_K^{eff} V/2|$
174 k_BT
Energy barrier
$M_S H_{K,in} V/2$

Fig. 4